Systematic Study: Channel Sounding via Modal Expansion

Alex J. Yuffa, Benjamin F. Jamroz, Jacob D. Rezac, Dylan F. Williams
National Institute of Standards and Technology
Boulder, CO 80305, USA
alex.yuffa@nist.gov

***Abstract*—We present a preliminary study of a modal (partial wave) expansion of the field used to characterize a propagation channel. We assume that the measurements of the scalar, two-dimensional field from which the modal expansion coefficients are obtained, contain Gaussian phase noise with zero mean. Three spatial sampling patterns of the field are considered. We find that the accuracy of the reconstructed field is strongly influenced by the spatial sampling pattern.**

I. Introduction

The use of robotics and optical tracking in RF measurements has created both new opportunities and challenges in the characterization of antennas and propagation channels. With these systems, it is possible to sample an RF field inside a volume while maintaining almost absolute control over the spatial positioning. For decades, antennas in the near field have been characterized via modal (partial wave) expansions, where the modal expansion coefficients are calculated from regularly spaced measurements on some canonical surface. Recently, these modal expansions have been used to characterize propagation channels [1]–[3] in order to accurately estimate the performance of advanced communications technology in complex environments.

A number of questions naturally arise when we use a modal expansion to characterize a propagation channel:

- How many modes should we keep in the expansion? What are the consequences of this on the condition number of the matrix that will need to be inverted to find the expansion coefficients?
- How should the RF field be spatially sampled? For example, should we sample the field on a canonical surface or is it better to sample the field throughout a volume? Should these samples be regularly or randomly spaced?
- How accurate should each measurement be in order to achieve an estimate of the expansion coefficients within a given tolerance?

The above questions are interdependent and, because of the large parameter space, answering them via computer simulations is a daunting task. Therefore, we present a systematic study of the above questions using the simplified model of scalar waves in two-dimensions.

Official contribution of the National Institute of Standards and Technology; not subject to copyright in the United States.

In this work, we assume that each measurement contains zero-mean Gaussian phase noise. Phase error can be representative of component level distortions including thermal effects, cable bending [4], and timing errors. Additionally, the spatial positioning errors will primarily manifest themselves in the phase measurements because the amplitude varies very little over small distances relative to wavelength λ. Incorporating realistic phase errors into our analysis allows a more direct comparison to existing channel measurements.

To the best of our knowledge, no such systematic study has been previously reported in the literature. Throughout this paper, we use the Système International (SI) unit system and assume that all fields are harmonic in time with a suppressed $\exp(-\mathrm{i}\omega t)$ time factor, where ω is the angular frequency.

II. Problem Formulation

Consider a disk region Ω of radius R that is source-free. Then, the total field $U(r,\theta)$ in Ω can be written as

$$U(r,\theta)=\sum_{n=-\infty}^{\infty} A_n J_n(kr)\mathrm{e}^{\mathrm{i}n\theta}, \tag{1}$$

where J_n is the integer order Bessel function of the first kind, k is the free-space wavenumber, and $(r\geq 0, -\pi\leq\theta<\pi)$ are the polar coordinates centered on Ω. In practical computations, the infinite sum in (1) must be truncated. One usually chooses to truncate the sum at $N\sim kR$ because $J_n(kr)$ decays rapidly when $n\geq kr$. In particular, we use the modified Wiscombe's criterion $N(\eta)$ [5], [6] to determine N; namely,

$$N(\eta)=\begin{cases}2, & 0<\eta<0.02\\ \lceil \eta+4\eta^{1/3}+1\rceil, & 0.02\leq\eta\leq 8\\ \lceil \eta+4.05\eta^{1/3}+2\rceil, & 8<\eta<4200\\ \lceil \eta+4\eta^{1/3}+2\rceil, & 4200\leq\eta\end{cases}, \tag{2}$$

where $\lceil\ \rceil$ denotes the ceiling function. If all of the measurements are taken on the boundary of Ω, then N is given by (2) with $\eta=kR$. However, if the measurement is taken at the point (r_m,θ_m), where $r_m<R$, then we terminate the sum at $N(kr_m)$. In other words, the unknown coefficients A_n are determined from a linear system

$$U(r_m,\theta_m)=\sum_{n=-N_m}^{N_m} A_n J_n(kr_m)\mathrm{e}^{\mathrm{i}n\theta_m}, \tag{3}$$

where $N_m = N(kr_m)$, $U(r_m, \theta_m)$ is the measured (known) field at the point (r_m, θ_m), and $m = 1, \ldots, M$. We solve the linear system (3) in the least squares sense assuring that a formal solution exists. Of course, if the measured data are too noisy and/or the number of measurements M is too small, then the least squares solution will produce a poor estimate of the field. In this case, we could consider a solution technique designed to operate well in the presence of noise, such as Tikhonov regularization. We note that terminating the sum in (3) based on the radial location of the measurement point instead of the boundary of Ω is important in order to maintain a reasonable condition number for the linear system. This is because the measurement at the radial distance r_m contains very little information about the expansion coefficients A_n, where $n > kr_m$ (recall that $J_n(kr_m) \approx 0$ when $n > kr_m$).

III. Results

We numerically study the method described in Sec. II by solving (3) in the least squares sense to obtain an approximation to the field $V(r, \theta)$. The field $V(r, \theta)$ is composed of 12 plane waves and is shown in Fig. 1. To avoid a possible source of confusion, we will refer to the field $V(r, \theta)$ as the "true" field in Ω.

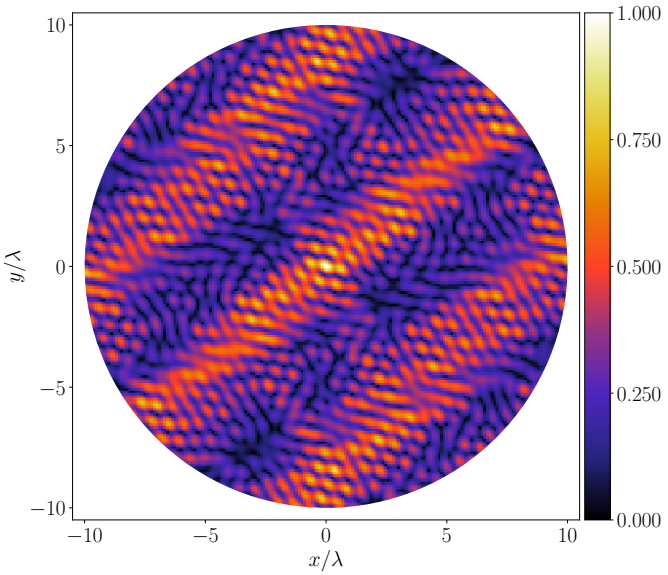

Fig. 1: (Color online) The amplitude (in arb. unit) of the true field $V(r, \theta) \in \Omega$ is shown as a function of $x = r\cos\theta$ and $y = r\sin\theta$.

Throughout the paper, we consider three spatial sampling patterns of the true field:

(i) a uniform Cartesian grid superimposed over Ω,
(ii) a set of Cartesian points (x_m, y_m) in Ω randomly drawn from a uniform distribution,
(iii) a set of points on the boundary of Ω separated by some angle $\triangle\theta$; i.e., $x_m = R\cos(m\triangle\theta)$ and $y_m = R\sin(m\triangle\theta)$.

We shall refer to these as uniform, random, and boundary sampling patterns, respectively.

The condition number of the matrix associated with (3) depends on the chosen spatial sampling pattern. The condition number for each of the spatial sampling patterns as a function of the sampling density is shown in Fig. 2. From the figure, we see that the three spatial sampling patterns have a similar condition number of $\sim 10^5$ if the field is estimated from a reasonable number of measurements. Thus, we conclude that the loss of precision caused by the numerical method used to solve the linear system is approximately the same for all three sampling patterns.

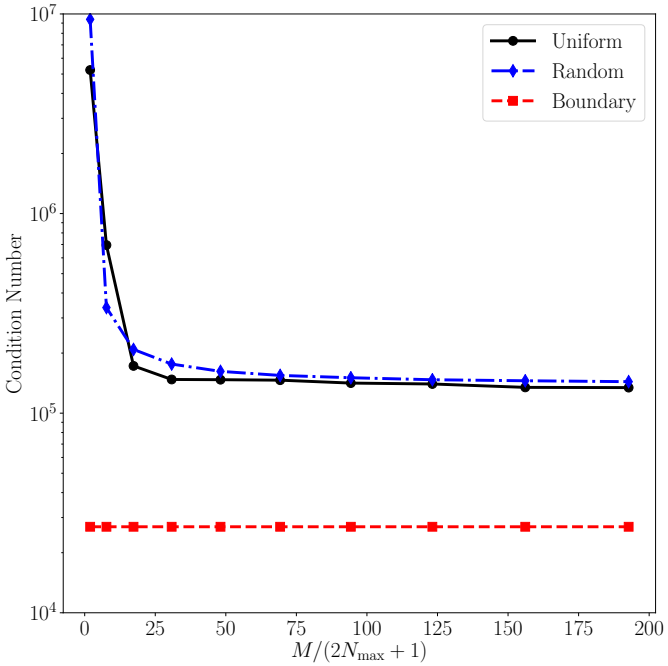

Fig. 2: (Color online) The condition number for uniform, random, and boundary sampling patterns is shown as a function of the sampling density.

We measure the accuracy of the reconstructed field $U(r, \theta)$ in terms of the number of significant digits it agrees with the true field $V(r, \theta)$. The number of the correct significant digits is approximated from the relative error via

$$\delta(r,\theta) = \begin{cases} -\log_{10}\frac{|U(r,\theta)-V(r,\theta)|}{|V(r,\theta)|} & \text{if} \quad |V(r,\theta)| > \epsilon \\ \text{undefined} & \text{if} \quad |V(r,\theta)| \le \epsilon \end{cases}, \quad (4)$$

where $\epsilon = 10^{-5/2}$ (50 dB). Figures 3–5 show the approximate number of the correct significant digits for each of the spatial sampling patterns when the measurement of the true field $V(r, \theta)$ contains 10° zero-mean Gaussian phase noise. The expansion coefficients A_n associated with Fig. 3 were calculated from $M = 1576$ measurement points; in the case of uniform sampling, this corresponds to sampling every 0.45λ. From Fig. 3, we see that the uniform and random sampling methods yield approximately the same results at this sampling density. We also see that the boundary sampling method performs the worst, especially near the the boundary of Ω. The expansion coefficients A_n associated with Fig. 4 and Fig. 5

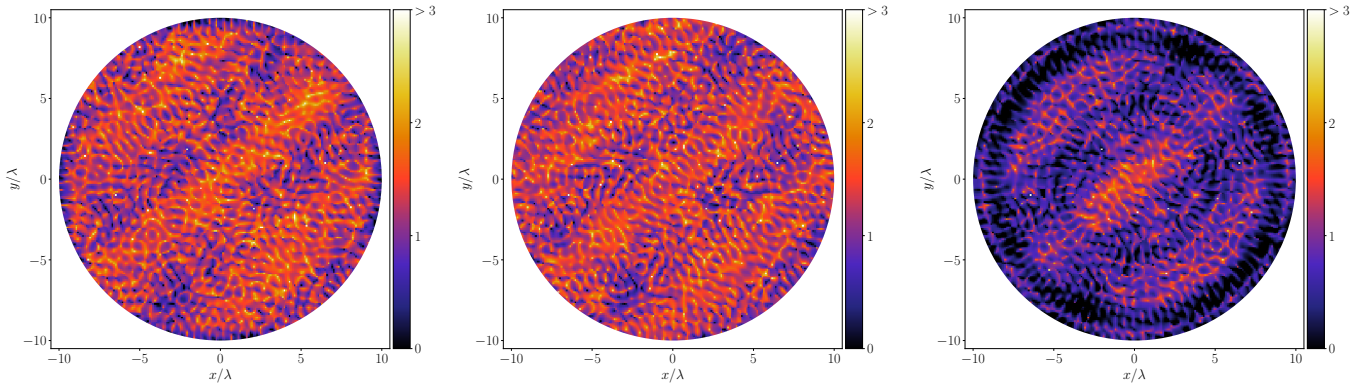

(a) Uniform sampling (b) Random sampling (c) Boundary sampling

Fig. 3: (Color online) The number of correct significant digits, δ, of the reconstructed field U is shown as a function of position. The expansion coefficients were calculated from $M = 1576$ measurements with 10° zero-mean Gaussian phase noise. In the uniform sampling case, this corresponds to sampling every 0.45λ.

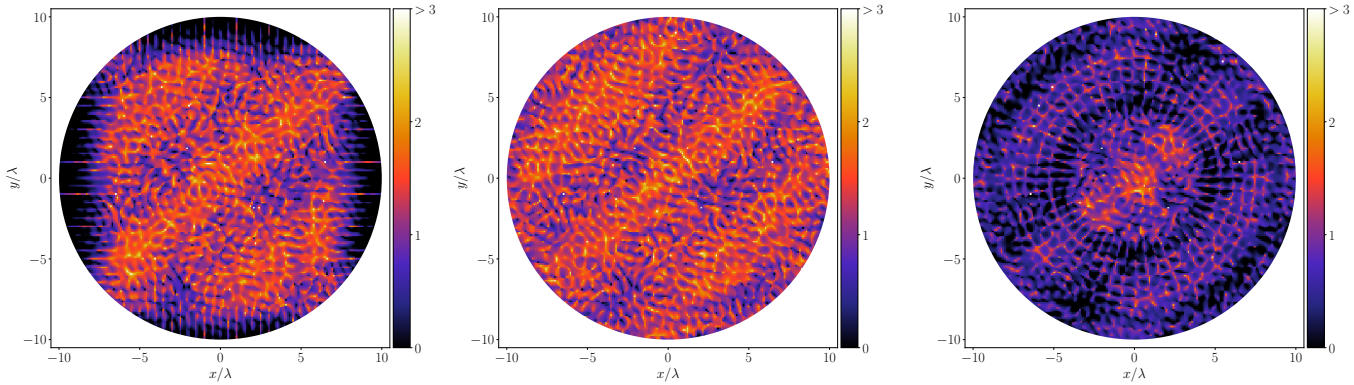

(a) Uniform sampling (b) Random sampling (c) Boundary sampling

Fig. 4: (Color online) The number of correct significant digits, δ, of the reconstructed field U is shown as a function of position. The expansion coefficients were calculated from $M = 1371$ measurements with 10° zero-mean Gaussian phase noise. In the uniform sampling case, this corresponds to sampling every 0.48λ.

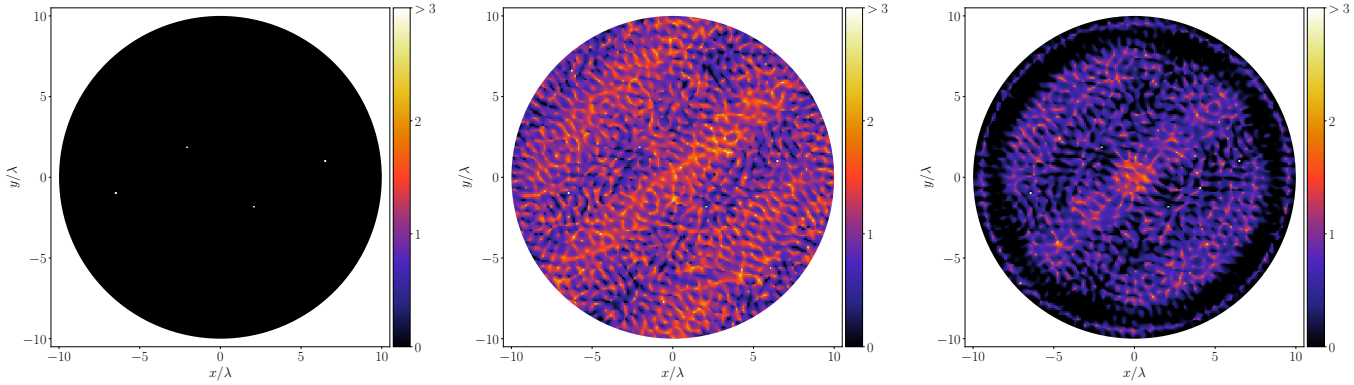

(a) Uniform sampling (b) Random sampling (c) Boundary sampling

Fig. 5: (Color online) The number of correct significant digits, δ, of the reconstructed field U is shown as a function of position. The expansion coefficients were calculated from $M = 1255$ measurements with 10° zero-mean Gaussian phase noise. In the uniform sampling case, this corresponds to sampling every $\lambda/2$.

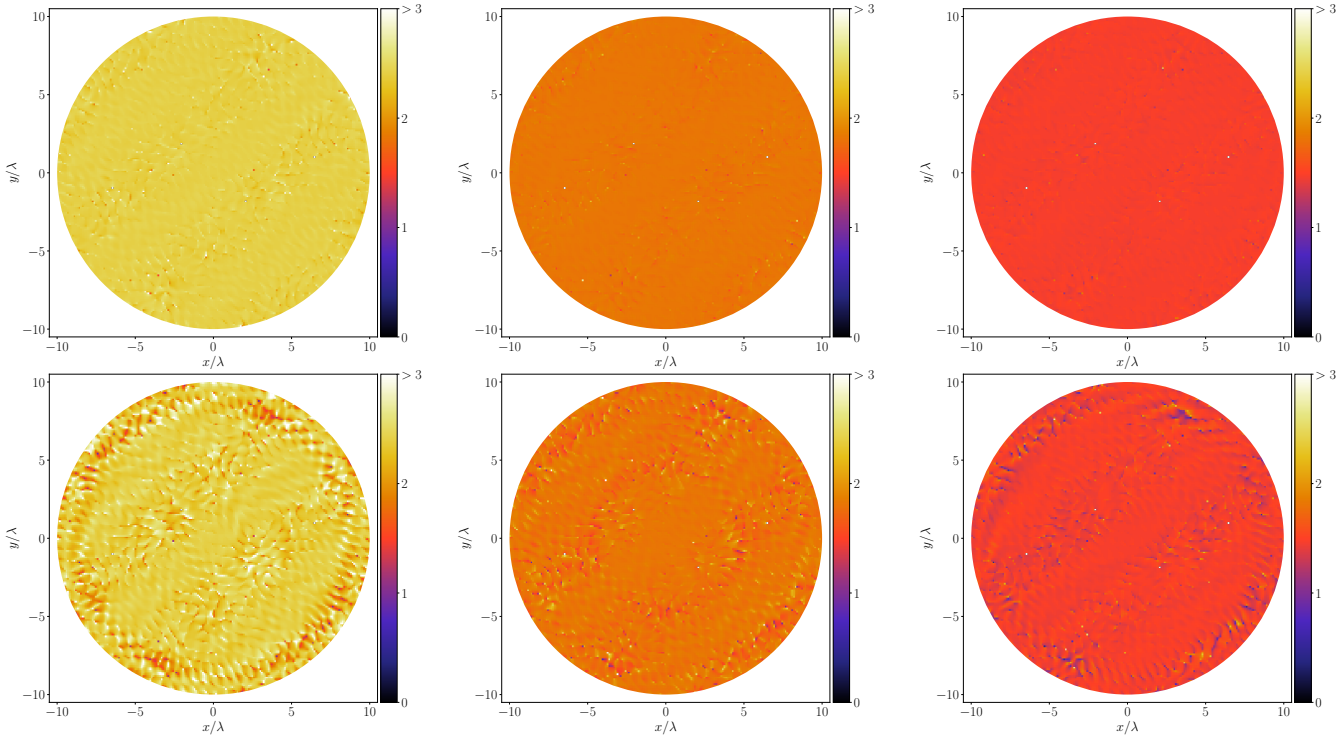

(a) 5° zero-mean Gaussian phase noise (b) 10° zero-mean Gaussian phase noise (c) 15° zero-mean Gaussian phase noise

Fig. 6: (Color online) The top (bottom) panel shows the expected number of correct significant digits, δ, of the reconstructed field U as a function of position for the random (boundary) sampling method at three phase noise levels: 5° (panel a), 10° (panel b), and 15° (panel c). The results shown are based on 10^4 Monte Carlo simulations with $M = 1255$.

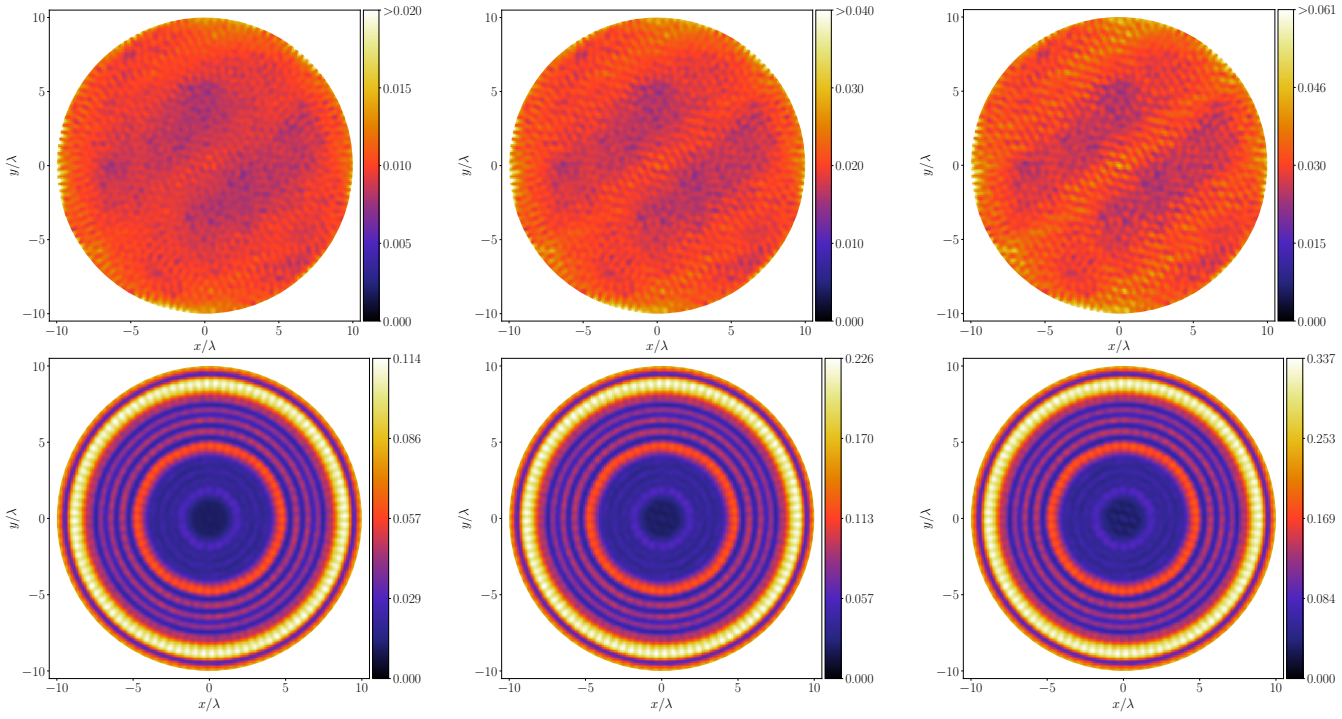

(a) 5° zero-mean Gaussian phase noise (b) 10° zero-mean Gaussian phase noise (c) 15° zero-mean Gaussian phase noise

Fig. 7: (Color online) The Monte Carlo sample standard deviation of the reconstructed field U associated with the Fig. 6 is shown as a function of position.

were calculated from $M = 1371$ and $M = 1255$ measurement points, respectively. In the case of uniform sampling, these sampling densities corresponds to sampling every 0.48λ and $\lambda/2$, respectively. From panel (a) in Figures 3–5, we see that the uniform sampling method is very sensitive to the sampling density and, generally speaking, it requires sampling more frequently than $\lambda/2$. In other words, the uniform sampling method deteriorates completely (zero-digit accuracy) when the sampling is at or below Nyquist sampling. However, from panels (b) and (c) in Figures 3–5, we see that the random and boundary sampling methods do not suffer from this highly sensitive dependence on the sampling density.

Figures 3–5 show the accuracy of the solution for one particular realization of random phase noise. However, these figures do not illustrate the expected (average) performance of each of the sampling methods. In Fig. 6, we show the expected (average) accuracy for the random and boundary spatial sampling methods (uniform sampling not shown because it yields zero-digit accuracy) computed from 10^4 Monte Carlo simulations for three levels of zero-mean Gaussian phase noise: $5^\circ, 10^\circ$ and 15°. Here, we see that the random spatial sampling is the most accurate. For the phase noise below 10°, the random spatial sampling yields two- to three- digit accuracy and for 15° phase noise it yields one- to two- digit accuracy. Notice that this accuracy is almost independent of the spatial position in Ω. This is in contrast with the boundary sampling where the accuracy tends to decrease near the boundary of Ω. Furthermore, the accuracy of the boundary sampling also appears to be correlated with the crests and troughs of the true field.

The Monte Carlo sample standard deviation values associated with the field in Fig. 6 are shown in Fig. 7. We see that the standard deviation of the field computed from the random sampling pattern is largely featureless and gradually increases with increasing phase noise. However, the standard deviation of the field computed from the boundary sampling pattern has a peculiar concentric ring structure. This ring structure suggests that the boundary sampling pattern is not robust with respect to the zero-mean Gaussian phase noise. Furthermore, the boundary sampling pattern yields noticeably higher standard deviation values, especially near the boundary of Ω (note scale of the colorbars in Fig. 7).

IV. Conclusions

We have analyzed the feasibility of using a modal (partial wave) expansion of the field to characterize a two-dimensional propagation channel. We only considered scalar waves and measurements with zero-mean Gaussian phase noise. Under these limiting assumptions, our results suggest that the RF field should be randomly sampled in the region of interest, Ω. If the field is sampled regularly in Ω, then our results indicate that the field must be sampled more densely than $\lambda/2$ to yield an accuracy comparable to the random sampling method. Although the accuracy of the field computed from the random and boundary sampling methods are similar, their associated standard deviations are not. In particular, the boundary sample methods produces noticeably larger standard deviations in a concentric ring pattern, see bottom panel in Fig. 7.

The analysis above was done by solving the linear system (3) in the least squares sense and by using the Wiscombe criterion to choose N_m for each measurement point. Thus, the work presented here also provides a benchmark for propagation channel characterization using modal expansions with a novel sampling-aware algorithm.

References

[1] A. Bernland, M. Gustafsson, C. Gustafson, and F. Tufvesson, "Estimation of spherical wave coefficients from 3-D positioner channel measurements," *IEEE Antennas Wirel. Propag. Lett.*, vol. 11, pp. 608–611, 2012.

[2] J. Naganawa, K. Haneda, M. Kim, T. Aoyagi, and J. Takada, "Antenna de-embedding in FDTD-based radio propagation prediction by using spherical wave function," *IEEE Trans. Antennas Propag.*, vol. 63, no. 6, pp. 2545–2557, 2015.

[3] Y. Miao, K. Haneda, M. Kim, and J. Takada, "Antenna de-embedding of radio propagation channel with truncated modes in the spherical vector wave domain," *IEEE Trans. Antennas Propag.*, vol. 63, no. 9, pp. 4100–4110, 2015.

[4] K. A. Remley, D. F. Williams, P. D. Hale, C.-M. Wang, J. Jargon, and Y. Park, "Millimeter-wave modulated-signal and error-vector-magnitude measurement with uncertainty," *IEEE Transactions on Microwave Theory and Techniques*, vol. 63, no. 5, pp. 1710–1720, May 2015.

[5] W. J. Wiscombe, "Improved Mie scattering algorithms," *Appl. Opt.*, vol. 19, no. 9, pp. 1505–1509, May 1980.

[6] A. A. R. Neves and D. Pisignano, "Effect of finite terms on the truncation error of Mie series," *Opt. Lett.*, vol. 37, no. 12, p. 2418, Jun. 2012.